Title

Trace Element Removal in Distributed Drinking Water Treatment Systems by Cathodic H2O2 Production and UV Photolysis

Journal

Environmental Science and Technology, 52(1)

ISSN

0013-936X

Authors

Barazesh, James M
Prasse, Carsten
Wenk, Jannis
et al.

Publication Date

2018-01-02

DOI

10.1021/acs.est.7b04396

Peer reviewed

Environmental Science & Technology

Article

Cite This: Environ. Sci. Technol. 2018, 52, 195−204

pubs.acs.org/est

Trace Element Removal in Distributed Drinking Water Treatment Systems by Cathodic H_2O_2 Production and UV Photolysis

James M. Barazesh,[†,‡] Carsten Prasse,[†] Jannis Wenk,[§] Stephanie Berg,[∥] Christina K. Remucal,[∥,⊥] and David L. Sedlak*[,†]

[†]Department of Civil and Environmental Engineering, University of California at Berkeley, Berkeley, California 94720 United States

[‡]Carollo Engineers, Inc., Costa Mesa, California 92626, United States

[§]Department of Chemical Engineering and Water Innovation & Research Centre, University of Bath, Claverton Down, Bath, BA2 7AY United Kingdom

[∥]Environmental Chemistry & Technology Program, University of Wisconsin-Madison, Madison, Wisconsin 53706 United States

[⊥]Department of Civil and Environmental Engineering, University of Wisconsin-Madison, Madison, Wisconsin 53706 United States

Supporting Information

ABSTRACT: As water scarcity intensifies, point-of-use and point-of-entry treatment may provide a means of exploiting locally available water resources that are currently considered to be unsafe for human consumption. Among the different classes of drinking water contaminants, toxic trace elements (e.g., arsenic and lead) pose substantial operational challenges for distributed drinking water treatment systems. Removal of toxic trace elements via adsorption onto iron oxides is an inexpensive and robust treatment method; however, the presence of metal-complexing ligands associated with natural organic matter (NOM) often prevents the formation of iron precipitates at the relatively low concentrations of dissolved iron typically present in natural water sources, thereby requiring the addition of iron which complicates the treatment process and results in a need to dispose of relatively large amounts of accumulated solids. A point-of-use treatment device consisting of a cathodic cell that produced hydrogen peroxide (H_2O_2) followed by an ultraviolet (UV) irradiation chamber was used to decrease colloid stabilization and metal-complexing capacity of NOM present in groundwater. Exposure to UV light altered NOM, converting ~6 μM of iron oxides into settable forms that removed between 0.5 and 1 μM of arsenic (As), lead (Pb), and copper (Cu) from solution via adsorption. After treatment, changes in NOM consistent with the loss of iron-complexing carboxylate ligands were observed, including decreases in UV absorbance and shifts in the molecular composition of NOM to higher H/C and lower O/C ratios. Chronoamperometric experiments conducted in synthetic groundwater revealed that the presence of Ca^{2+} and Mg^{2+} inhibited intramolecular charge-transfer within photoexcited NOM, leading to substantially increased removal of iron and trace elements.

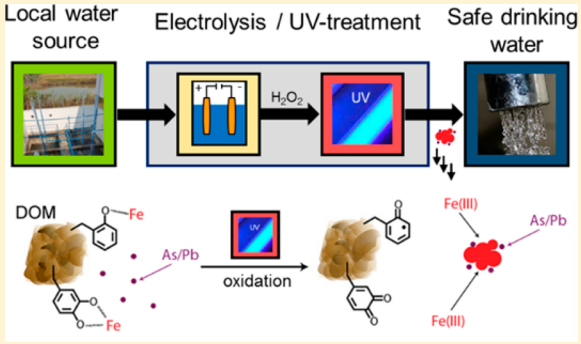

INTRODUCTION

Inadequate access to clean drinking water is a globally pervasive problem. Amidst rapid population growth, urbanization, and climate change, water demand exceeds available freshwater resources in many locations.[1,2] Continued reliance on difficult-to-maintain, energy-intensive centralized water treatment and conveyance systems may not be a viable option, especially in an era when reduction in energy and greenhouse gas emissions is a high priority.[3,4] For example, the energy use associated with pumping water over the Tehachapi Mountains in southern California is approximately 2.4 kWh m^{-3}, which is comparable to the energy required for seawater desalination.[5] New water resource management strategies are needed to reliably provide potable water to cities and to reduce the energy use associated with importing, treating, and distributing water from centralized treatment facilities.

Small scale, point-of-use and point-of-entry drinking water treatment systems may facilitate the use of nontraditional water sources, such as roof water, stormwater, and water from shallow aquifers. Such systems are particularly attractive in new developments because they can be installed rapidly without the significant capital costs required for centralized facilities.[4,6] Despite their attractiveness, the presence of trace concentrations of organic contaminants (e.g., pesticides, solvents, pharmaceuticals), toxic trace elements (e.g., arsenic, lead), and waterborne pathogens questions the viability of distributed drinking water treatment systems if they cannot provide

Received: August 27, 2017
Revised: October 31, 2017
Accepted: November 30, 2017
Published: December 14, 2017

DOI: 10.1021/acs.est.7b04396
Environ. Sci. Technol. 2018, 52, 195−204

adequate treatment and disinfection needed for potable use.[7,8] Challenges associated with the transport, storage, and use of chemicals typically employed in conventional drinking water treatment, such as chlorine, activated carbon, and alum, limit the types of processes that can be employed in distributed water systems.[9] Widespread adoption of decentralized drinking water treatment will require cost-effective, reliable technologies capable of operating without frequent maintenance or the need to replenish chemical reagents.

Electrolysis and ultraviolet (UV) treatment are well suited for distributed drinking water treatment systems due to their small footprint, flexible design, and intrinsic advantages of low cost and lack of chemical consumption. For example, we recently developed a device capable of treating up to 250 L d^{-1} of water contaminated by trace organic contaminants by employing cathodically driven electrolysis for hydrogen peroxide (H_2O_2) production followed by UV photolysis with a modest energy consumption (~3−7 kWh log^{-1} m^{-3}).[10] The UV fluence delivered by the systems (~3000 mJ cm^{-2}) was sufficient to disinfect most source waters. However, the ability of the system to remove trace elements was not evaluated.

Technologies for removing trace elements from drinking water include oxidation, coagulation, precipitation, ion exchange, and membrane-based methods.[11−13] Among these, coprecipitation or adsorption onto iron oxides is frequently used because it is cost-effective and simple to operate. Although effective, this approach poses technical challenges with respect to management and disposal of contaminated solids generated from iron addition, especially in distributed water treatment systems.[14−17] Under conditions encountered in groundwater or in natural organic matter (NOM)-containing surface waters, relatively high doses of iron (i.e., > 100 μM) are typically needed to remove oxyanions and metals due to the presence of iron-complexing ligands in NOM that decrease the mineral saturation index and inhibit iron oxide precipitation.[18,19]

Previous research has demonstrated that photochemical reactions alter the structure of NOM in a manner that lowers its affinity for Fe(III).[18−20] Although the rates of sunlight photolysis of NOM and Fe(III)−NOM complexes in natural waters are relatively slow, the application of low pressure Hg lamps (λ = 254 nm) results in higher rates in engineered treatment systems (Supporting Information (SI) Figure S1).[21] Despite previous efforts to describe photochemical reactions of iron and organic matter in natural systems,[22,23] the potential for exploiting these processes to enhance iron oxide precipitation and trace element removal during water treatment has not been considered.

The objective of this research was to evaluate the potential of using cathodically produced H_2O_2 and UV light to enhance the removal of dissolved trace elements in the presence of NOM and low concentrations of iron (i.e., ~ 15 μM). The simultaneous removal of arsenic, lead, and copper was investigated. Arsenic was selected due to importance as an ubiquitous geogenic contaminant.[24] Lead and copper were chosen due to concerns about metal leaching from water distribution systems. To assess the role of solution conditions on the process, experiments were performed in authentic groundwater as well as synthetic groundwater containing varying concentrations of NOM and divalent cations (e.g., Ca^{2+}, Mg^{2+}). The treatment-induced alterations of NOM were investigated by quantifying changes in electronic absorption spectra, intramolecular electron transfer properties, and mass spectra.

MATERIALS AND METHODS

Chemicals. All experiments were performed with reagent grade $NaHCO_3$, NaCl, NaBr; ACS grade trace elements ($Pb(NO_3)_2$, $CuCl_2$, Na_3AsO_3); and alkali earth metals ($Ca(NO_3)_2$, $Mg(NO_3)_2$) obtained from Sigma-Aldrich (St. Louis, MO). Suwannee River natural organic matter (2R101N) obtained from the International Humic Substances Society served as model groundwater NOM as it is a well-characterized and frequently employed isolate. Stock solutions of trace metals (100 μM in 1% HNO_3; pH ≈ 1.7) and anoxic stock solutions of ferrous iron ($FeSO_4$; 100 mM) were used to prevent precipitation and/or metal oxidation prior to addition to solutions. The addition of trace elements from acidic stock solutions lowered the initial pH of solutions by approximately 0.5 units. UV photolysis of NO_3^- counterions increased the rate of formation of hydroxyl radical ($HO^\bullet$) by less than 0.2% relative to $HO^\bullet$ formed from the photolysis of H_2O_2 generated in the cathode (SI Section 2.1).

Solutions. Experiments were conducted with arsenic-contaminated groundwater collected from Colusa County, California (Table 1). To elucidate the role of different solutes on metal redox reactions and complexation, additional experiments were conducted with a synthetic groundwater solution prepared in Milli-Q water with added NOM and major ions (i.e., Na^+, Ca^{2+}, Mg^{2+}, Fe^{2+}, HCO_3^-, Cl^-, and Br^-) at concentrations comparable to those detected in the authentic groundwater. In some experiments, concentrations of Ca^{2+} and Mg^{2+}, Fe^{2+}, or NOM were varied. Synthetic groundwater solutions were amended with 1 μM of dissolved As(III), Pb(II), and Cu(II) from acidic stock solutions, whereas authentic groundwater typically contained approximately 0.4 μM of As and was modified with only 1 μM of dissolved Pb(II) and Cu(II).

Table 1. Composition of Authentic and Synthetic Matrices

ion	colusa county groundwater	synthetic groundwater
Ca^{2+} (μM)	273.5 ± 0.35	0−250
Mg^{2+} (μM)	272 ± 0.96	0−250
SO_4^{2-} (μM)	33.1 ± 0.42	0
Cl^- (μM)	240 ± 7.2	500
Br^- (μM)	0.6 ± 0.09	0.5
PO_4^{3-} (μM)	510 ± 120	0
SiO_2 (μM)	700 ± 245	0
DIC (mM)[a]	5.84 ± 0.03	5
DOC (mgC L^{-1})[b]	0.44 ± 0.17	0.5
pH	7.3 ± 0.2	7.8
DO[c] (μM)	69 ± 18	250
Trace Element		
Fe (μM)	11.0 ± 2.7	10
As (μM)	0.36 ± 0.03	1
Cu (μM)	0.07 ± 0.02	1
Pb (μM)	0.01 ± 0.0	1

[a]Dissolved inorganic carbon ([HCO_3^-] + [CO_3^{2-}]). [b]Dissolved organic carbon [c]Dissolved oxygen

Photolysis and Electrolysis Experiments. Experiments to assess trace element removal were performed in a previously described point-of-use treatment system.[10] The device consisted of dual-chambered electrolysis cell employing a carbon-based gas-permeable cathode to generate H_2O_2 from ambient air directly in the solution prior to exposure to low-pressure UV irradiation (G23 Odyssea Pool Lamp, 9W) in a

DOI: 10.1021/acs.est.7b04396
Environ. Sci. Technol. 2018, 52, 195−204

batch reactor (see SI Section 2.2 for cathode fabrication). After UV treatment, the water passed through an anode chamber (Figure 1). Samples (10 mL) for analysis of pH, H_2O_2, UV−visible absorbance, and trace elements were collected prior to treatment and after each treatment step starting approximately 30 min after treatment was initiated. Under the constant current densities (25 A m^{-2}; $\varphi_{observed}$ = 13.6 V vs SHE) and system flow rate (121 L d^{-1}) used in these experiments, 510 ± 41 μM of H_2O_2 was produced in the solution (i.e., the Coulombic efficiency was 86%).[10] Subsequent UV irradiation (I_{254}° = 0.107 mEi m^2 s^{-1}; F_0 ∼ 3000 mJ cm^{-2}) resulted in photolysis of approximately 35% of the electrochemically generated H_2O_2[10] as well as other photolytic processes (e.g., photolysis of NOM and Fe(III)−NOM complexes to generate photochemically produced reactive intermediates).[21,22,25]

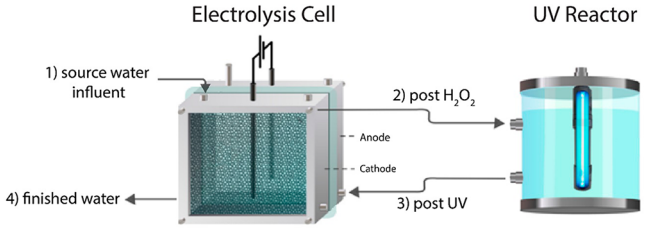

Figure 1. Sample collection locations and flow through the modular advanced oxidation treatment system combining a dual-chambered electrolysis cell and UV lamp.

To differentiate between the effects of H_2O_2 photolysis and other processes, a series of experiments were performed with a stainless-steel cathode that reduced O_2 to H_2O without producing substantial concentrations of H_2O_2 (i.e., $[H_2O_2]$ < 1 μM). Experiments were also conducted in the presence of selective quenchers of reactive oxygen species and excited triplet states of NOM, including tertiary butanol (1 mM), sodium azide (NaN_3; 50 μM) and isoprene (500 μM) to scavenge $HO^{\bullet}$, $^1O_2$, and ^{3}NOM, respectively.[21−23,25−27] Sodium azide and isoprene were selected due to their hydrophilic nature, low reactivity with H_2O_2, and minimal light absorption at 254 nm (SI Figure S2 and Section 2.3).[23] Superoxide radical ($O_2^{-\bullet}$) was assumed to play an insignificant role in photochemical processes due to its catalytic dismutation in the presence of elevated concentrations of dissolved Cu^{2+}.[26,27]

NOM Characterization by Mass Spectrometry. NOM chemical composition was evaluated by Fourier transform-ion cyclotron resonance mass spectrometry (FT-ICR MS). To prepare samples, NOM was concentrated using solid phase extraction (SPE) as described previously.[28] Approximately 250 mL of sample was acidified to pH 2 ± 0.1 using 1 M HCl. Acidified samples were passed through Agilent Bond Elut-PPL cartridges (500 mg; 6 mL) that had been washed with methanol. Following extraction, the cartridges were rinsed with 0.01 M HCl and air-dried. DOM was eluted with 2 mL of methanol and stored in the dark at 4 °C.

Samples were diluted 1:10 in a 60:40 acetonitrile:Milli-Q matrix and introduced into a SolariX XR 12T FT-ICR MS (Bruker) via a Triversa NanoMate sample delivery system (Advian). The accumulation time was set to 0.01 s for each sample and 350 scans were collected. The gas pressure was 0.3 psi and −1.4 kV was applied for the electrospray.

Peaks over a range from 200 to 600 m/z and a relative intensity of 0.0001% were exported to R for processing. Nominal masses of peaks were determined by adding the mass of a proton and a linear calibration was applied, as described previously.[29] Formulas containing C, H, O, and ^{13}C were considered for matching. For a formula assignment to be considered successful, the error had to be less than 0.2 ppm and it had to be part of a homologous series with more than three members (CH_4 versus O or ± CH_2).[30−32] Weighted averages of NOM molecular weight, H/C ratio, and O/C ratio were calculated using the peak intensity and the molecular weight, H/C ratio, or O/C ratio of a given chemical formula, respectively (see SI Section 2.4 for calculations).

Optical and Electrochemical Properties of Fe−NOM complexes. To quantify changes in the molecular composition of NOM during treatment, authentic and synthetic groundwater samples were filtered and UV−visible absorption spectra was analyzed at each sampling location in the treatment system. Samples were adjusted to pH 9.0 using concentrated NaOH prior to measurement of spectra from 240 to 500 nm. To assess light absorption solely by NOM, absorption due to Ca^{2+}, Mg^{2+}, H_2O_2, and NO_3^- was subtracted from the spectra prior to analysis (SI Figure S3 and Section 2.5). Differential absorbance spectra (Δabs) were calculated by subtracting specific absorbance (i.e., $A(\lambda)$) between the influent (i.e., untreated water) and effluent (i.e., postanode). Spectral slope coefficients of the NOM absorbance spectra were calculated by nonlinear least-squares fitting of a single exponential model between 275 and 295 nm ($S_{275-295}$) and between 240 and 500 nm ($S_{240-500}$). Changes in spectral slopes and differential absorption spectra were used in conjunction with data on chemical composition determined by FT-ICR MS to assess shifts in NOM aromaticity and apparent molecular weight during treatment, as described previously.[33−35] Additional details of the data analysis are provided in SI Section 2.5.

To characterize the redox properties of NOM and metal−NOM complexes, cyclic voltammograms (CVs) were collected in anhydrous dimethyl sulfoxide (DMSO; 50 mL) containing 5 mM tetrabutylammonium hexafluorophosphate (NBu_4PF_6) as the supporting electrolyte. Experiments were performed in a 3-electrode setup employing Pt wires as the working and counter electrodes (0.25 mm diameter) along with a nonaqueous Ag/Ag^+ reference electrode (BASi).[36] Experiments were performed at a scan rate of 10 mV s^{-1} starting from the open-circuit potential (∼0 to −0.1 V) and scanned cathodically over a 2 V potential range. CVs were collected for electrolytes containing Suwannee River NOM (90 mg L^{-1}; ∼ 45 mgC L^{-1})[37] in the presence of 1 mM $Ca(Cl)_2$, $Mg(Cl)_2$, and/or $Fe(Cl)_3$. Spectra were corrected for the background spectra of DMSO. Prior to each CV, electrodes were sonicated in 50:50 CH_3OH/H_2O and electrolytes were purged with argon to remove O_2. The ferrocene/ferrocenium and benzoquinone/hydroquinone redox couples were used as reference reactions to validate the methodology and electrode response in the aprotic solvents.[36]

In addition, linear sweep voltammetry was employed to determine if trace element removal occurred via sorption and direct reduction on the cathode. Voltammograms indicated that the reduction of O_2 to H_2O_2 was the main reduction reaction and direct trace metal reduction was negligible at the potentials employed in the experiments (SI Figure S4 and Section 2.6).

To investigate the importance of ligand-to-metal charge transfer (LMCT) photoreduction reactions, solutions of synthetic groundwater containing NOM (1 mg L^{-1}; ∼ 0.5

DOI: 10.1021/acs.est.7b04396
Environ. Sci. Technol. 2018, 52, 195−204

mgC L^{-1}) were irradiated with UV light in batch experiments conducted in the presence of the Fe(II)-complexing compound, ferrozine (FZ_3; 100 μM).[18,20,38] Fe(II) production was quantified in the presence and absence of Ca^{2+} and Mg^{2+}. Production rates of the Fe(II)−FZ_3 complex from Fe(III)−NOM were determined spectroscopically at 562 nm and corrected for light screening by FZ_3 ($\varepsilon_{FZ3,\lambda=254\ nm}$ = 12900 M^{-1} cm^{-1}; SI Figure S5 and Section 2.7).[39] Experiments were performed at pH 6.5 to minimize oxidation of Fe(II) by O_2 prior to complexation of the metal by ferrozine (see SI Section 2.8).

Analytical Methods. H_2O_2, dissolved organic carbon, and dissolved inorganic carbon were measured using standard methods.[40] Unfiltered and filtered (0.22 μm nylon filters) water samples for measurement of total and dissolved As, Cu, Fe, and Pb, respectively, were digested with 1% HNO_3 prior to analysis by inductively coupled plasma mass spectrometry (ICP-MS, Agilent). Absorption spectra were recorded with a UV-2600 spectrophotometer (Shimadzu) using 1 cm quartz cuvettes. Spectral irradiance of the UV lamp (G23 Odyssea Pool Lamp, 9W) and a collimated beam Oriel solar simulator (Spectra Physics 91194) were measured with a spectroradiometer (RPS 380, international light). Br^-, Cl^-, PO_4^{3-}, and SO_4^{2-} were analyzed using a Dionex DX-120 ion chromatograph with an AS19G column. Ca^{2+} and Mg^{2+} were analyzed by ICP-MS. Fluence was determined by chemical actinometry using 10 μM atrazine (ε_{254} = 3860 M^{-1} cm^{-1}, ϕ_{254} = 0.046 mol Ei^{-1}) in 1 mM borate buffer (pH 8).[10] Atrazine was quantified by multiple reaction monitoring (MRM) mode with an Agilent 1200 series HPLC system coupled to a 6460 triple quadrupole tandem mass spectrometer (HPLC-MS/MS).

RESULTS AND DISCUSSION

Speciation and Fate of Iron and Trace Elements during Treatment. The presence of NOM in groundwater matrices resulted in dissolved iron concentrations that exceeded predicted solubility. Separation of cathodic (i.e., production of H_2O_2) and anodic (i.e., production of O_2) redox reactions via the cation exchange membrane led to significant fluctuations of pH during the treatment process: influent (7.8 ± 0.2), postcathode (pH 9.3 ± 0.3), post-UV (pH 9.1 ± 0.3) and postanode (pH 7.7 ± 0.2). Over this pH range, the predicted equilibrium solubility of inorganic Fe(III) ranges from 0.008 μM to 0.064 μM.[41] As a result, in experiments employing synthetic groundwater in the absence of organic matter, nearly all the iron (i.e., $[Fe]_{initial}$ ~ 10 μM) was converted to filterable forms (i.e., amorphous $Fe(OH)_{3(s)}$) due to the rapid oxidation of Fe(II) by O_2 and subsequent precipitation of supersaturated Fe(III) (i.e., $[Fe]_{dissolved}$ = 0.182 ± 0.05 μM; SI Figure S6). Conversely, in synthetic and authentic groundwater matrices containing approximately 0.5 mgC L^{-1} organic matter and 10.5 μM of iron, roughly 60% of the Fe in the influent water passed through a 0.22 μm filter (Figure 2A). Significantly higher concentrations of dissolved iron compared to thermodynamically predicted concentrations indicated either the formation of soluble Fe(III)−NOM complexes or stabilization of submicron colloids by NOM and inhibition of particle aggregation.[19,42] Metal complexation is mediated through multidentate coordination by ligands present in humic substances,[43] resulting in Fe-binding capacities between 2.1 and 240 nmol mg^{-1} NOM.[20] Thus, at the metal/NOM concentration ratios observed in authentic and synthetic matrices (i.e., 15 000 nmol mg^{-1}), NOM likely adsorbed onto the surface of nucleated amorphous

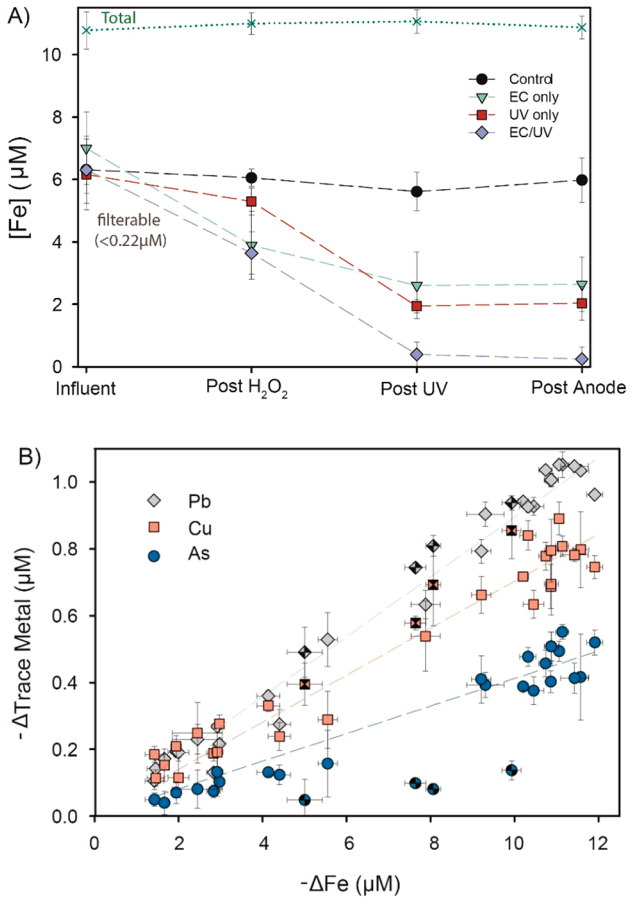

Figure 2. (A) Concentration of dissolved and total (i.e., dissolved and colloidal) Fe during treatment of authentic groundwater under different reactor configurations. (B) Correlation between Fe removal with Pb, Cu, and As removal observed for synthetic (solid symbols) and authentic matrices (checked symbols). Dashed lines correspond to linear regressions of the synthetic matrix results. Error bars represent ± one standard deviation of triplicate experiments.

$Fe(OH)_3$ nanoclusters and inhibited polymerization and formation of solids that could be filtered out by a 0.22 μm filter. Complexation of iron in the trivalent oxidation state was consistent with the higher stability constants of NOM with Fe(III) (log β ~ 40−49) relative to Fe(II) (log β ~ 13) and supported by the absence of Fe(II)−FZ_3 when ferrozine was added to the water (data not shown).[44,45]

In the absence of applied current or UV light (i.e., control conditions), iron removed by filtration (i.e., approximately 4.5 μM) did not change as authentic groundwater passed through the treatment system (Figure 2A). Exposure of authentic groundwater to the electrochemical system operating in the absence of UV light (i.e., EC only) resulted in the formation of an additional 4 μM of Fe that could be removed by filtration. Although the oxidation of iron-chelating catecholate moieties (E_H° = +0.84 V)[46] by H_2O_2 (E_H° ($H_2O_2/HO_2^\bullet$) = +1.51 V)[47] is thermodynamically feasible, these reactions are usually slow (~2 M^{-1} s^{-1}).[48] Therefore, the simultaneous increased Fe removal and loss of H_2O_2 (i.e., 58 ± 17 μM; SI Figure S7) observed in dark experiments conducted in the absence of UV irradiation may be attributable to oxidation of less abundant, high affinity metal-binding functional groups (i.e., amines and thiols) by H_2O_2,[19] or the decomposition of H_2O_2 on the surface of iron colloids yielding reactive $HO^\bullet$ capable of oxidizing Fe-

DOI: 10.1021/acs.est.7b04396
Environ. Sci. Technol. 2018, 52, 195−204

coordinating moieties.[49] Similar conversion of Fe to filterable forms (i.e., formation of 4 μM of Fe that could be removed by filtrations) was observed when authentic groundwater was irradiated with UV light in the absence of H_2O_2 (i.e., UV only; experiments conducted with a stainless steel cathode) as well as control experiments performed in the absence of current (i.e., no pH increase), indicating that phototransformation of Fe−NOM complexes were not affected by an increase in pH from 7.8 to 9.3 (SI Figure S8). Simultaneous electrochemical and photochemical treatment (i.e., EC/UV) resulted in nearly complete conversion of the Fe into forms that were removed by filtration. Analysis of unfiltered samples of authentic groundwater subjected to electrochemical and UV treatment and allowed to settle overnight revealed approximately 90% removal of total Fe (i.e., dissolved and colloidal) from the solution (SI Figure S9). Therefore, the term removal refers to the conversion of Fe and trace elements into particulate forms that can be filtered out of solution or separated by sedimentation given sufficient holding time.

Linear correlations were observed between the increase in Fe removal and the removal of trace elements from solution (Figure 2B). Pb was most efficiently removed (mol_{Pb}:mol_{Fe} of 0.089 ± 0.007), followed by Cu (mol_{Cu}:mol_{Fe} of 0.070 ± 0.005) and As (mol_{As}:mol_{Fe} of 0.041 ± 0.009). For Pb^{2+} and Cu^{2+}, no difference was observed between experiments conducted in authentic (checkered symbols) and simulated groundwater (solid symbols) despite variability in their composition, suggesting that adsorption or coprecipitation was not influenced by other solutes such as and phosphate. In contrast, As removal decreased substantially (i.e., decrease in mol_{As}:mol_{Fe} by −70%) in authentic groundwater, likely due to competition between oxyanions for metal adsorption sites on hydrous ferric oxide precipitates.[50,51]

Photochemical Transformation of NOM. As described above, cathodically produced H_2O_2 and photochemical reactions alter natural organic matter in a manner that decreases its ability to prevent formation and/or stabilize Fe(III)-oxide particles. To gain insight into the mechanisms that led to the transformation of the NOM complexes, experiments were repeated in synthetic groundwater. Although reactions with H_2O_2 contributed to Fe removal in authentic groundwater, its effect on Fe removal was absent in synthetic matrices (SI Figure S10; post-H_2O_2). While the reason for this discrepancy is unknown, oxidation of NOM induced by H_2O_2 likely varies among NOM sources. Because UV photolysis showed the same effect in both the authentic and synthetic matrices and the photoreactivity of NOM has been well documented,[22,52] changes in NOM during UV treatment were investigated in detail.

To determine the relative contributions of direct and indirect photolysis to the changes in NOM and iron upon UV irradiation, a series of experiments were conducted in which reactive intermediates (i.e., $HO^{\bullet}$, $^1O_2$, ^{3}NOM) produced by photoexcitation of NOM or H_2O_2, as well as ligand and light-mediated Fenton process (i.e., photo-Fenton), were scavenged (SI Figure S11). Experiments conducted with a stainless steel cathode (i.e., no production of H_2O_2) or in the presence of 1 mM tertiary butanol (i.e., enough to reduce $[HO^{\bullet}]_{SS}$ by approximately 70%) revealed no change in Fe removal, indicating that reactions with $HO^{\bullet}$ were not important (see SI Section 3.6 for calculations). Although the potential contribution of $HO^{\bullet}$ to Fe removal was hypothesized as an explanation for results from dark experiments, its negligible role in irradiated solutions is not unsurprising given the significant light screening by NOM (~82%), low molar absorptivity of H_2O_2 at 254 nm (ε_{254} = 18.6 M^{-1} cm^{-1}), and limited fraction of $HO^{\bullet}$ reacting with NOM (i.e., ~ 12%) in the presence of other solutes (i.e., H_2O_2, HCO_3^-, CO_3^{2-}; see SI Section 3.7 for calculations). Similarly, the presence of both 50 μM NaN_3 and 500 μM isoprene, enough to lower $[^1O_2]_{SS}$ and $[^3NOM]_{SS}$ by 17% and 50%, respectively, did not influence Fe removal. Collectively, these results suggest that direct photolysis of NOM was responsible for conversion of organically complexed Fe and aggregation of NOM-stabilized iron oxide nanoclusters into forms that were removed upon filtration.

Changes in the molecular composition and optical properties of NOM exposed to UV irradiation was assessed by FT-ICR MS and UV−visible spectroscopy. Analysis of FT-ICR MS data revealed 1455 chemical formulas in irradiated and nonirradiated authentic groundwater, of which 763 (i.e., 52%) of the peaks were common to both, 248 (i.e., 17%) peaks were observed only in the nonirradiated solution, and 444 (i.e., 31%) peaks were unique to the irradiated solution (SI Table S5). Although interpretation of FT-ICR data requires caution because not all carbon is retained by SPE and only compounds amenable to ionization (e.g., carboxylic acids) are detected, and thus the method only captures a subset of the total chemical formulas,[53] results can provide insight into the changes in chemical composition that occurred during irradiation. For example, photolysis of authentic groundwater decreased the average apparent molecular weight of detected peaks from 399.5 to 346.9 Da, with a greater loss of intensity for higher molecular weight formulas common to both dark and light-exposed solutions (Figure 3A). Similarly, approximately 70% of the peaks that completely disappeared upon UV irradiation were in the high molecular weight fraction (i.e., > 500 Da; SI Figure S12). The apparent decreases in molecular weight upon irradiation are in agreement with an increase in spectral slope values (i.e., $S_{240-500}$ and $S_{275-295}$; SI Figure S13).[34,35] Absorbance loss over the entire UV−visible spectrum (i.e., photobleaching; SI Figure S14), shifts in chemical compositions to slightly higher H/C ratios (Figure 3B), and decreases in double bond equivalents (i.e., 9.40 to 8.71; SI Table S9) were consistent with ring cleavage or loss of aromaticity of chromophores.[54,55]

Mass spectral shifts in NOM to lower O/C ratios (i.e., average 0.063 lower) following exposure to UV irradiation provided additional insights into the photooxidation of Fe−NOM complexes (Figure 3B). Photochemical loss of carboxyl moieties to produce hydrocarbons and CO_2 results in a 2:1 ratio of oxygen to carbon loss.[54] Due to the fact that carboxylate[45,56] and structurally similar α-hydroxy acid moieties[57] are the dominant metal-coordinating functional groups in NOM, the shifts in chemical composition observed upon UV irradiation are consistent with a photodecarboxylation mechanism previously proposed by Ward and Cory.[54] Furthermore, the binding strength of organic matter onto iron nanoparticle surfaces has been positively correlated with carboxyl concentration.[58,59] Consequently, oxidation of Fe-coordinating carboxylate moieties following exposure of Fe(III)−NOM complexes to UV light likely decreases specific Fe-complexing ability and weakens NOM binding to mineral surfaces, resulting in colloid aggregation. To test this hypothesis, previously treated synthetic groundwater was filtered, amended with 10 μM Fe(II), and subjected to a second pass through the treatment system (SI Figure S15).

DOI: 10.1021/acs.est.7b04396
Environ. Sci. Technol. 2018, 52, 195−204

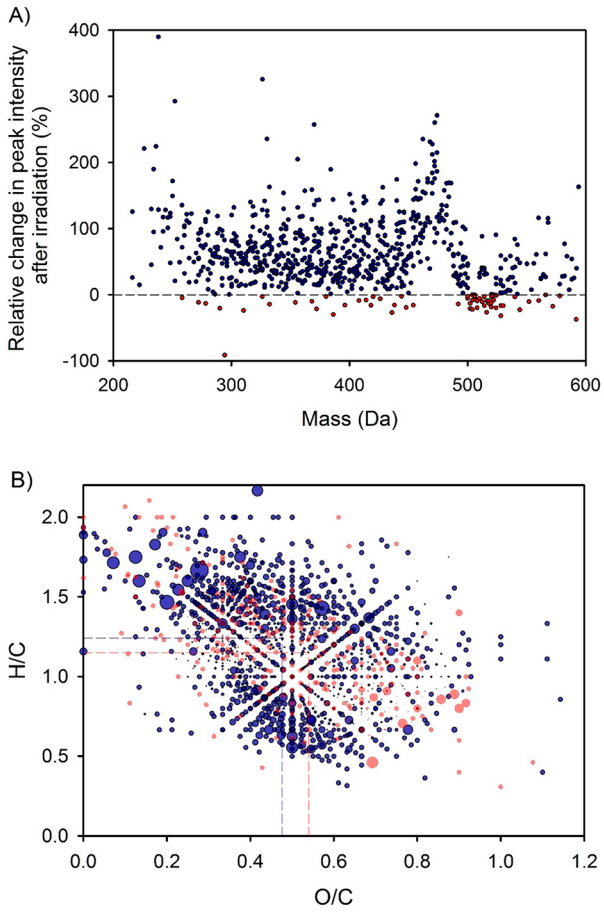

Figure 3. (A) Loss (red circles) or gain (blue circles) in relative peak intensity after UV irradiation of authentic groundwater. Only chemical formulas common to both the unirradiated and irradiated solution are depicted. (B) van Krevelen diagrams of chemical formulas that were either unique to the nonirradiated authentic groundwater or decreased in intensity following irradiation (red circles) or were unique to the irradiated solution or increased in intensity following irradiation (blue circles). Bubble size is proportional to the peak intensity. Dashed lines correspond to the weighted average H/C and O/C ratios.

Results from UV−visible spectroscopy indicate that although NOM is present (SI Figure S16), filterable dissolved iron concentrations at all sampling locations were indistinguishable from control experiments performed with synthetic groundwater in the absence of NOM (SI Table S4), confirming an irreversible loss of Fe(III)-binding ability and reduction in bulk organic stabilizing ability after the first exposure to UV light.

Effect of Solution Chemistry on Phototransformation of Fe(III)−NOM Complexes. Divalent cations (e.g., Ca^{2+}, Mg^{2+}) can impact iron oxide structural conformation, surface charge, as well as photolability of organically complexed iron.[60] For example, Ca^{2+} and Mg^{2+} promote the photochemical reduction of Fe(III)−EDTA complexes (i.e., LMCT reactions) via formation of ternary complexes that increase the quantum yield.[20] Treatment experiments performed in synthetic groundwater indicated that Fe removal increased with increasing concentrations of Ca^{2+} and Mg^{2+} (Figure 4). The possible role of divalent cation bridging of Fe(III)−NOM complexes[61] or metal exchange[20] of Ca^{2+} and Mg^{2+} with Fe(III) at NOM complexation sites was assessed. Similar uptake of Ca^{2+} and Mg^{2+} (~40 μM of each cation) in the presence and absence of NOM suggests that Fe removal via divalent cation bridging of

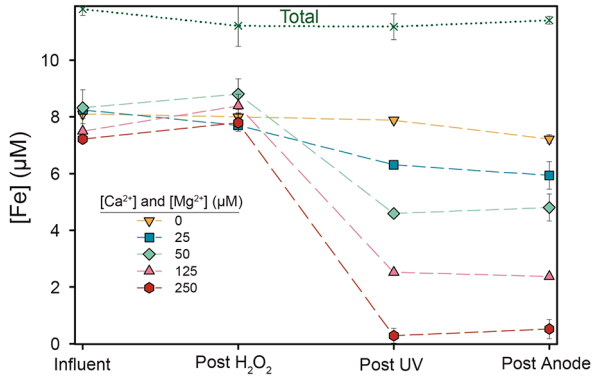

Figure 4. Concentration of dissolved and total (i.e., dissolved and colloidal) Fe in synthetic groundwater exposed to the combined EC/UV treatment system at varying concentrations of Ca^{2+} and Mg^{2+} (0 to 250 μM). Error bars represent ±1 standard deviation of triplicate experiments.

Fe(III)−NOM complexes was not important (SI Figure S17). In addition, increased Fe loss via metal exchange between Ca^{2+} and Mg^{2+} with Fe(III)−NOM complexes was deemed unimportant because Fe removal in dark experiments was not affected by the presence of divalent cations (SI Figure S18). Comparison of photodegradation experiments performed in synthetic groundwater revealed more rapid shifts in NOM chemical composition to aliphatic formulas (i.e., higher H/C ratios; SI Tables S8 and S9), more pronounced shifts in the distribution of peak intensities to lower molecular weight formulas (SI Figure S19), and greater UV−visible absorbance loss (SI Figures S20−S23) in the presence of Ca^{2+} and Mg^{2+}, consistent with the hypothesis that divalent cations increased the changes in NOM that occurred upon UV irradiation.

The enhanced photoreactivity of NOM may be attributable to conformational changes induced by divalent cation complexation that either accelerates LMCT reactions, resulting in the formation of Fe(II) and oxidation of the NOM-complexing functional group,[18−20,38] or alteration of intramolecular charge transfer reactions of NOM which decreased light absorption and/or quantum yield.[22,62−64] To provide insight into the governing mechanism, photochemical formation of Fe(II) and electron transfer kinetics were analyzed in the synthetic groundwater matrix. Initial photochemical production rates of Fe(II) under UV irradiation approached 4.42 ± 0.4 nM s^{-1} (SI Figure S24). Considering the hydraulic conditions (i.e., 1.8 CSTRs-in-series) and residence time (~660 s) in the UV reactor during continuous treatment, approximately 3 μM of Fe(III) should have been reduced and subsequently oxidized to produce particulate Fe(III)-oxides. This is, however, less than half of the iron that was actually removed in the system. Furthermore, comparable Fe(II) production rates in the presence and absence of Ca^{2+} and Mg^{2+} do not support the hypothesis that divalent cations accelerate rates of the LMCT reactions (Figure 4). These findings are similar to results of experiments conducted with Suwannee River fulvic acid, in which divalent cations did not affect production of Fe(II) under solar photolysis conditions.[20,38]

Intramolecular electron transfer between photoexcited acceptor moieties (i.e., carbonyls) and ground-state donor moieties (i.e., phenolates) stabilizes NOM and slows phototransformation rates.[63,65,66] Conformational changes of the NOM structure by Ca^{2+} or Mg^{2+} complexation can disrupt this donor−acceptor electronic coupling,[67] leading to accelerated

DOI: 10.1021/acs.est.7b04396
Environ. Sci. Technol. 2018, 52, 195−204

phototransformation of NOM. To evaluate this hypothesis, cyclic voltammetry experiments were performed using NOM, Fe−NOM, and Fe−NOM with added Ca^{2+} and Mg^{2+} (Figure 5). Although weakly defined, voltammograms for Suwannee

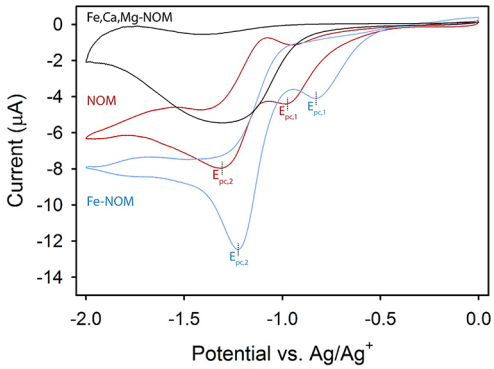

Figure 5. Cyclic voltammograms of Suwannee River NOM (90 mg L^{-1}; ~ 45 mgC L^{-1}), Suwannee River NOM with 50 μM $Fe(Cl)_3$, and Suwannee River NOM with 50 μM $Fe(Cl)_3$, 500 μM $Ca(Cl)_2$, and 500 μM $Mg(Cl)_2$. E_{pc} refers to the cathodic peak potential.

River NOM contained a pair of cathodic peaks at −0.98 V and −1.32 V, which were consistent with the peak reduction potentials for *p*-benzoquinone (SI Figure S24). Thus, these peaks correspond to single electron reduction reactions to form an intermediate semiquinone radical ($E_{pc,1}$ = −0.75 V) and a quinone dianion ($E_{pc,2}$ = −1.33 V).[36] Addition of Fe^{2+} to the NOM solution shifted the onset potential of the cathodic waves to more positive potentials ($\Delta E_{pc,1}$ = +0.140 V; $\Delta E_{pc,2}$ = +0.048 V) and increased the redox activity relative to the free ligand wave (i.e., NOM only).[68] In the presence of Ca^{2+} and Mg^{2+}, however, reductive currents decreased and the second reduction peak disappeared. These results suggest inhibition of charge-transfer pathways between redox-active functional groups due to the formation of a divalent cation-semiquinone complex,[67,69] suppressing intramolecular electron transfer and accelerating the phototransformation of NOM (SI Figure S25). These results, combined with those from spectroscopic and compositional analysis, provide evidence that divalent cations increased the photolability of the organic matter.

Environmental Significance. Drinking water sources that are candidates for treatment by point-of-use devices will frequently contain iron, alkaline earth metals (e.g., Ca^{2+} and Mg^{2+}), and natural organic matter at concentrations comparable to those studied here. The biogeochemistry of the source water, however, will dictate the chemical speciation and redox state of iron as well as the nature of trace elements present; contamination of groundwaters typically involves the reductive dissolution of iron hydroxides, resulting in simultaneous release of arsenic and Fe(II) under anoxic conditions,[70,71] while dissolved iron is often present as organically complexed Fe(III) in oxygenated surface waters which may be contaminated with Cu and Pb from the corrosion of galvanized pipes.[72,73] The technology described here is a simple, low-cost option for distributed treatment of arsenic-, copper-, and lead-contaminated waters under these conditions. For example, the U.S. Geological Survey recently measured dissolved iron concentrations in over 7000 arsenic-contaminated groundwater wells in California (SI Figure S27). The concentration of iron in the authentic groundwater employed in this study fell within the 87th percentile of the monitoring data, indicating that such concentrations are relatively common.

Considering only the electrical energy demand from the electrochemical cell and UV lamp, the treatment of water had an energy demand of 2.2 kWh m^{-3}, comparable to values determined for UV/H_2O_2 treatment needed to transform trace organic contaminants in different surface and wastewaters (i.e., between 0.17 and 2.28 kWh m^{-3}).[74] Similarly, this device nearly completely removed a suite of trace organic contaminants[10] from the authentic groundwater, whereas it removed 12 of the initial 28 μg L^{-1} of As (See SI Section 3.13 for calculations). Thus, considering an As sorption capacity of 0.012 mol As per mol iron oxide (Figure 2B), treating authentic groundwater containing 28 μg L^{-1} to below the World Health Organization Maximum Contaminant Level of 10 μg L^{-1} would require an additional dosing of 6.7 μM Fe. Irrespective of the source of the Fe, the system would only generate 1.1 mg of waste sludge per liter of water treated, which is less than sludge produced in iron electrocoagulation based treatment for the remediation of As (5−137 mg L^{-1}; see SI Section 3.14 for calculations).[75,76] Challenges still remain in the development of a low-cost means of separating contaminant-laden iron oxides after treatment by gravitational settling and/or membrane filtration.

In addition to providing a standalone distributed treatment system, this research may offer substantial promise for decreasing operational costs and increasing process efficiency of iron-based electrocoagulation techniques by reducing electrolysis times, iron dosing, and sludge production simply though the integration of a UV treatment step. The treatment system might also be applicable to other problematic trace elements in groundwaters known to be removable with iron-based treatment approaches such as antimony,[77] selenium,[78] and chromium.[79] Macromolecular structure, binding capacity, and physicochemical properties of NOM are affected by solution chemistry,[19] and therefore additional research is needed to assess the effectiveness of the treatment system and behavior of metal−NOM complexes under varying pH values, metal-to-NOM ratios, and molecular compositions of organic matter.

■ ASSOCIATED CONTENT

Supporting Information

The Supporting Information is available free of charge on the ACS Publications website at DOI: 10.1021/acs.est.7b04396.

Details of the calculations about the composition of authentic and synthetic groundwaters, cathode fabrication, electronic absorption spectra of water constituents, spectral slope calculations, photochemical ferrous iron production, system energy demand, and calculations on the steady-state concentrations of reactive intermediates in addition to supporting tables and figures referenced in this work (PDF)

■ AUTHOR INFORMATION

Corresponding Author

*E-mail: sedlak@berkeley.edu.

ORCID

Jannis Wenk: 0000-0001-9182-0407
Christina K. Remucal: 0000-0003-4285-7638
David L. Sedlak: 0000-0003-1686-8464

DOI: 10.1021/acs.est.7b04396
Environ. Sci. Technol. 2018, 52, 195−204

Notes

The authors declare no competing financial interest.

■ ACKNOWLEDGMENTS

This study was supported by the U.S. National Institute for Environmental Health Sciences (NIEHS) Superfund Research Program (Grant P42 ES004705) and the Superfund Research Center at University of California, Berkeley. The authors would like to acknowledge the UW-Madison Human Proteomics Program Mass Spectrometry Facility (initially funded by the Wisconsin partnership funds) for support in obtaining mass spectrometry data and NIH S10OD018475 for the acquisition of ultrahigh resolution mass spectrometer for biomedical research. We thank Siva RS Bandaru for his invaluable help and feedback in the preparation of this manuscript.

■ REFERENCES

(1) Hering, J. G.; Waite, T. D.; Luthy, R. G.; Drewes, J. E.; Sedlak, D. L. A Changing Framework for Urban Water Systems. *Environ. Sci. Technol.* **2013**, *47* (19), 10721−10726.

(2) Vörösmarty, C. J.; Green, P.; Salisbury, J.; Lammers, R. B. Global Water Resources: Vulnerability from Climate Change and Population Growth. *Science* **2000**, *289* (5477), 284−288.

(3) Liu, Y.; Hejazi, M.; Kyle, P.; Kim, S. H.; Davies, E.; Miralles, D. G.; Teuling, A. J.; He, Y.; Niyogi, D. Global and Regional Evaluation of Energy for Water. *Environ. Sci. Technol.* **2016**, *50* (17), 9736−9745.

(4) Larsen, T. A.; Hoffmann, S.; Lüthi, C.; Truffer, B.; Maurer, M. Emerging solutions to the water challenges of an urbanizing world. *Science* **2016**, *352* (6288), 928−933.

(5) Nair, S.; George, B.; Malano, H. M.; Arora, M.; Nawarathna, B. Water-energy-greenhouse gas nexus of urban water systems: Review of concepts, state-of-art and methods. *Resources Conservation and Recycling* **2014**, *89*, 1−10.

(6) Dahlgren, E.; Göçmen, C.; Lackner, K.; van Ryzin, G. Small Modular Infrastructure. *Engineering Economist* **2013**, *58* (4), 231−264.

(7) Benotti, M. J.; Trenholm, R. A.; Vanderford, B. J.; Holady, J. C.; Stanford, B. D.; Snyder, S. A. Pharmaceuticals and endocrine disrupting compounds in U.S. drinking water. *Environ. Sci. Technol.* **2008**, *43* (3), 597−603.

(8) Schwarzenbach, R. P.; Escher, B. I.; Fenner, K.; Hofstetter, T. B.; Johnson, C. A.; von Gunten, U.; Wehrli, B. The Challenge of Micropollutants in Aquatic Systems. *Science* **2006**, *313* (5790), 1072−1077.

(9) Larsen, A. T.; Udert, K. M.; Lienert, J. Source separation and decentralization for wastewater management. *IWA Publishing* **2013**, *12*, 491.

(10) Barazesh, J. M.; Hennebel, T.; Jasper, J. T.; Sedlak, D. L. Modular Advanced Oxidation Process Enabled by Cathodic Hydrogen Peroxide Production. *Environ. Sci. Technol.* **2015**, *49* (12), 7391−7399.

(11) Mohan, D.; Pittman, C. U. Arsenic removal from water/wastewater using adsorbents—a critical review. *J. Hazard. Mater.* **2007**, *142* (1), 1−53.

(12) Crittenden, J. C.; Trussell, R. R.; Hand, D. W.; Howe, K. J.; Tchobanoglous, G. *MWH's Water Treatment: Principles and Design*; John Wiley & Sons, 2012.

(13) Jekei, M.; Seith, R. Comparison of conventional and new techniques for removal of arsenic in a full scale water treatment plant. *Water Supply* **2000**, *18* (1/2), 628−631.

(14) McKenzie, R. The adsorption of lead and other heavy metals on oxides of manganese and iron. *Aust. J. Soil Res.* **1980**, *18* (1), 61−73.

(15) Dixit, S.; Hering, J. G. Comparison of Arsenic(V) and Arsenic(III) Sorption onto Iron Oxide Minerals: Implications for Arsenic Mobility. *Environ. Sci. Technol.* **2003**, *37* (18), 4182−4189.

(16) van Genuchten, C. M.; Addy, S. E. A.; Peña, J.; Gadgil, A. J. Removing Arsenic from Synthetic Groundwater with Iron Electrocoagulation: An Fe and As K-Edge EXAFS Study. *Environ. Sci. Technol.* **2012**, *46* (2), 986−994.

(17) Hering, J. G.; Katsoyiannis, I. A.; Theoduloz, G. A.; Berg, M.; Hug, S. J. Arsenic removal from drinking water: Experiences with technologies and constraints in practice. American Society of Civil Engineers, *J. Environ. Eng.***2017**.*14*30311700210.1061/(ASCE)EE.1943-7870.0001225

(18) Barbeau, K. Photochemistry of Organic Iron(III) Complexing Ligands in Oceanic Systems. *Photochem. Photobiol.* **2006**, *82* (6), 1505−1516.

(19) Aiken, G. R.; Hsu-Kim, H.; Ryan, J. N. Influence of Dissolved Organic Matter on the Environmental Fate of Metals, Nanoparticles, and Colloids. *Environ. Sci. Technol.* **2011**, *45* (8), 3196−3201.

(20) Fujii, M.; Yeung, A. C. Y.; Waite, T. D. Competitive Effects of Calcium and Magnesium Ions on the Photochemical Transformation and Associated Cellular Uptake of Iron by the Freshwater Cyanobacterial Phytoplankton Microcystis aeruginosa. *Environ. Sci. Technol.* **2015**, *49* (15), 9133−9142.

(21) Lester, Y.; Sharpless, C. M.; Mamane, H.; Linden, K. G. Production of Photo-oxidants by Dissolved Organic Matter During UV Water Treatment. *Environ. Sci. Technol.* **2013**, *47* (20), 11726−11733.

(22) Sharpless, C. M.; Aeschbacher, M.; Page, S. E.; Wenk, J.; Sander, M.; McNeill, K. Photooxidation-Induced Changes in Optical, Electrochemical, and Photochemical Properties of Humic Substances. *Environ. Sci. Technol.* **2014**, *48* (5), 2688−2696.

(23) Rosario-Ortiz, F. L.; Canonica, S. Probe compounds to assess the photochemical activity of dissolved organic matter. *Environ. Sci. Technol.*; **2016**.*5*01253210.1021/acs.est.6b02776

(24) Smedley, P. L.; Kinniburgh, D. G. A review of the source, behaviour and distribution of arsenic in natural waters. *Appl. Geochem.* **2002**, *17* (5), 517−568.

(25) Wenk, J.; von Gunten, U.; Canonica, S. Effect of Dissolved Organic Matter on the Transformation of Contaminants Induced by Excited Triplet States and the Hydroxyl Radical. *Environ. Sci. Technol.* **2011**, *45* (4), 1334−1340.

(26) Zafiriou, O. C.; Voelker, B. M.; Sedlak, D. L. Chemistry of the Superoxide Radical (O2-) in Seawater: Reactions with Inorganic Copper Complexes. *J. Phys. Chem. A* **1998**, *102* (28), 5693−5700.

(27) Goldstone, J. V.; Voelker, B. M. Chemistry of Superoxide Radical in Seawater: CDOM Associated Sink of Superoxide in Coastal Waters. *Environ. Sci. Technol.* **2000**, *34* (6), 1043−1048.

(28) Dittmar, T.; Koch, B.; Hertkorn, N.; Kattner, G. A simple and efficient method for the solid-phase extraction of dissolved organic matter (SPE-DOM) from seawater. *Limnol. Oceanogr.: Methods* **2008**, *6*, 230−235.

(29) Maizel, A. C.; Remucal, C. K. The effect of advanced secondary municipal wastewater treatment on the molecular composition of dissolved organic matter. *Water Res.* **2017**, *122*, 42−52.

(30) Koch, B. P.; Dittmar, T.; Witt, M.; Kattner, G. Fundamentals of molecular formula assignment to ultrahigh resolution mass data of natural organic matter. *Anal. Chem.* **2007**, *79* (4), 1758−1763.

(31) Kujawinski, E. B.; Behn, M. D. Automated analysis of electrospray ionization Fourier transform ion cyclotron resonance mass spectra of natural organic matter. *Anal. Chem.* **2006**, *78* (13), 4363−4373.

(32) Maizel, A. C.; Li, J.; Remucal, C. K. Relationships Between Dissolved Organic Matter Composition and Photochemistry in Lakes of Diverse Trophic Status, *Environ. Sci. Technol.*, **2017**.*5*1962410.1021/acs.est.7b01270

(33) Twardowski, M. S.; Boss, E.; Sullivan, J. M.; Donaghay, P. L. Modeling the spectral shape of absorption by chromophoric dissolved organic matter. *Mar. Chem.* **2004**, *89* (1−4), 69−88.

(34) Wenk, J.; Aeschbacher, M.; Salhi, E.; Canonica, S.; von Gunten, U.; Sander, M. Chemical Oxidation of Dissolved Organic Matter by Chlorine Dioxide, Chlorine, And Ozone: Effects on Its Optical and Antioxidant Properties. *Environ. Sci. Technol.* **2013**, *47* (19), 11147−11156.

(35) Helms, J. R.; Stubbins, A.; Ritchie, J. D.; Minor, E. C.; Kieber, D. J.; Mopper, K. Absorption spectral slopes and slope ratios as indicators

DOI: 10.1021/acs.est.7b04396
Environ. Sci. Technol. 2018, 52, 195−204

of molecular weight, source, and photobleaching of chromophoric dissolved organic matter. *Limnol. Oceanogr.* **2008**, *53* (3), 955−969.
(36) Nurmi, J. T.; Tratnyek, P. G. Electrochemical Properties of Natural Organic Matter (NOM), Fractions of NOM, and Model Biogeochemical Electron Shuttles. *Environ. Sci. Technol.* **2002**, *36* (4), 617−624.
(37) Appiani, E.; Page, S. E.; McNeill, K. On the Use of Hydroxyl Radical Kinetics to Assess the Number-Average Molecular Weight of Dissolved Organic Matter. *Environ. Sci. Technol.* **2014**, *48* (20), 11794−11802.
(38) Fujii, M.; Rose, A. L.; Waite, T. D.; Omura, T. Effect of divalent cations on the kinetics of Fe(III) complexation by organic ligands in natural waters. *Geochim. Cosmochim. Acta* **2008**, *72* (5), 1335−1349.
(39) Viollier, E.; Inglett, P. W.; Hunter, K.; Roychoudhury, A. N.; Van Cappellen, P. The ferrozine method revisited: Fe(II)/Fe(III) determination in natural waters. *Appl. Geochem.* **2000**, *15* (6), 785−790.
(40) American Public Health, A.; Eaton, A. D.; American Water Works, A.; Water Environment, F. *Standard Methods for the Examination of Water and Wastewater*; APHA-AWWA-WEF: Washington, D.C., 2005.
(41) Benjamin, M. M. *Water Chemistry*; Waveland Press, 2014.
(42) Neil, C. W.; Ray, J. R.; Lee, B.; Jun, Y.-S. Fractal aggregation and disaggregation of newly formed iron (III)(hydr) oxide nanoparticles in the presence of natural organic matter and arsenic. *Environ. Sci.: Nano* **2016**, *3* (3), 647−656.
(43) Baken, S.; Degryse, F.; Verheyen, L.; Merckx, R.; Smolders, E. Metal complexation properties of freshwater dissolved organic matter are explained by its aromaticity and by anthropogenic ligands. *Environ. Sci. Technol.* **2011**, *45* (7), 2584−2590.
(44) Rose, A. L. Effect of Dissolved Natural Organic Matter on the Kinetics of Ferrous Iron Oxygenation in Seawater. *Environ. Sci. Technol.* **2003**, *37* (21), 4877−4886.
(45) Milne, C. J.; Kinniburgh, D. G.; van Riemsdijk, W. H.; Tipping, E. Generic NICA−Donnan Model Parameters for Metal-Ion Binding by Humic Substances. *Environ. Sci. Technol.* **2003**, *37* (5), 958−971.
(46) Steenken, S.; Neta, P. One-electron redox potentials of phenols. Hydroxy- and aminophenols and related compounds of biological interest. *J. Phys. Chem.* **1982**, *86* (18), 3661−3667.
(47) CRC Handbook of Chemistry and Physics, 87th ed.; Lide, D. R., Ed.; National Institute of Standards and Technology. *J. Am. Chem. Soc.* 2007, *129*, (3), 724−724.
(48) Brunmark, A.; Cadenas, E. Electronically excited state generation during the reaction of p-benzoquinone with H2O2: Relation to product formation: 2-OH-and 2, 3-epoxy-p-benzoquinone the effect of glutathione. *Free Radical Biol. Med.* **1987**, *3* (3), 169−180.
(49) Kwan, W. P.; Voelker, B. M. Decomposition of hydrogen peroxide and organic compounds in the presence of dissolved iron and ferrihydrite. *Environ. Sci. Technol.* **2002**, *36* (7), 1467−1476.
(50) Rose, J.; Flank, A.-M.; Masion, A.; Bottero, J.-Y.; Elmerich, P. Nucleation and growth mechanisms of Fe oxyhydroxide in the presence of PO4 ions. 2. P K-edge EXAFS study. *Langmuir* **1997**, *13* (6), 1827−1834.
(51) Doelsch, E.; Rose, J.; Masion, A.; Bottero, J. Y.; Nahon, D.; Bertsch, P. M. Speciation and crystal chemistry of iron (III) chloride hydrolyzed in the presence of SiO4 ligands. 1. An Fe K-edge EXAFS study. *Langmuir* **2000**, *16* (10), 4726−4731.
(52) Del Vecchio, R.; Blough, N. V. Photobleaching of chromophoric dissolved organic matter in natural waters: kinetics and modeling. *Mar. Chem.* **2002**, *78* (4), 231−253.
(53) Stenson, A. C.; Landing, W. M.; Marshall, A. G.; Cooper, W. T. Ionization and fragmentation of humic substances in electrospray ionization Fourier transform-ion cyclotron resonance mass spectrometry. *Anal. Chem.* **2002**, *74* (17), 4397−4409.
(54) Ward, C. P.; Cory, R. M. Complete and Partial Photo-oxidation of Dissolved Organic Matter Draining Permafrost Soils. *Environ. Sci. Technol.* **2016**, *50* (7), 3545−3553.
(55) Maizel, A. C.; Remucal, C. K. Molecular Composition and Photochemical Reactivity of Size-Fractionated Dissolved Organic Matter. *Environ. Sci. Technol.* **2017**, *51* (4), 2113−2123.
(56) Kinniburgh, D. G.; Milne, C. J.; Benedetti, M. F.; Pinheiro, J. P.; Filius, J.; Koopal, L. K.; Van Riemsdijk, W. H. Metal Ion Binding by Humic Acid: Application of the NICA-Donnan Model. *Environ. Sci. Technol.* **1996**, *30* (5), 1687−1698.
(57) Faust, B. C.; Zepp, R. G. Photochemistry of aqueous iron(III)-polycarboxylate complexes: roles in the chemistry of atmospheric and surface waters. *Environ. Sci. Technol.* **1993**, *27* (12), 2517−2522.
(58) Strehlau, J. H.; Stemig, M. S.; Penn, R. L.; Arnold, W. A. Facet-dependent oxidative goethite growth as a function of aqueous solution conditions. *Environ. Sci. Technol.* **2016**, *50* (19), 10406−10412.
(59) Vindedahl, A. M.; Stemig, M. S.; Arnold, W. A.; Penn, R. L. Character of humic substances as a predictor for goethite nanoparticle reactivity and aggregation. *Environ. Sci. Technol.* **2016**, *50* (3), 1200−1208.
(60) van Genuchten, C. M.; Pena, J.; Amrose, S. E.; Gadgil, A. J. Structure of Fe(III) precipitates generated by the electrolytic dissolution of Fe(0) in the presence of groundwater ions. *Geochim. Cosmochim. Acta* **2014**, *127*, 285−304.
(61) Delaire, C.; van Genuchten, C. M.; Nelson, K. L.; Amrose, S. E.; Gadgil, A. J. Escherichia coli Attenuation by Fe Electrocoagulation in Synthetic Bengal Groundwater: Effect of pH and Natural Organic Matter. *Environ. Sci. Technol.* **2015**, *49* (16), 9945−9953.
(62) Aeschbacher, M.; Graf, C.; Schwarzenbach, R. P.; Sander, M. Antioxidant Properties of Humic Substances. *Environ. Sci. Technol.* **2012**, *46* (9), 4916−4925.
(63) Sharpless, C. M.; Blough, N. V. The importance of charge-transfer interactions in determining chromophoric dissolved organic matter (CDOM) optical and photochemical properties. *Environmental Science: Processes & Impacts* **2014**, *16* (4), 654−671.
(64) McKay, G.; Couch, K. D.; Mezyk, S. P.; Rosario-Ortiz, F. L. Investigation of the coupled effects of molecular weight and charge-transfer interactions on the optical and photochemical properties of dissolved organic matter. *Environ. Sci. Technol.* **2016**, *50* (15), 8093−8102.
(65) Parker, K. M.; Pignatello, J. J.; Mitch, W. A. Influence of Ionic Strength on Triplet-State Natural Organic Matter Loss by Energy Transfer and Electron Transfer Pathways. *Environ. Sci. Technol.* **2013**, *47* (19), 10987−10994.
(66) Boyle, E. S.; Guerriero, N.; Thiallet, A.; Vecchio, R. D.; Blough, N. V. Optical properties of humic substances and CDOM: relation to structure. *Environ. Sci. Technol.* **2009**, *43* (7), 2262−2268.
(67) Sato, A.; Takagi, K.; Kano, K.; Kato, N.; Duine, J. A.; Ikeda, T. Ca(2+) stabilizes the semiquinone radical of pyrroloquinoline quinone. *Biochem. J.* **2001**, *357* (Pt3), 893−898.
(68) Fimmen, R. L.; Cory, R. M.; Chin, Y.-P.; Trouts, T. D.; McKnight, D. M. Probing the oxidation−reduction properties of terrestrially and microbially derived dissolved organic matter. *Geochim. Cosmochim. Acta* **2007**, *71* (12), 3003−3015.
(69) Yuasa, J.; Suenobu, T.; Fukuzumi, S. Binding Modes in Metal Ion Complexes of Quinones and Semiquinone Radical Anions: Electron-Transfer Reactivity. *ChemPhysChem* **2006**, *7* (4), 942−954.
(70) McArthur, J.; Banerjee, D.; Hudson-Edwards, K.; Mishra, R.; Purohit, R.; Ravenscroft, P.; Cronin, A.; Howarth, R.; Chatterjee, A.; Talukder, T. Natural organic matter in sedimentary basins and its relation to arsenic in anoxic ground water: the example of West Bengal and its worldwide implications. *Appl. Geochem.* **2004**, *19* (8), 1255−1293.
(71) Hug, S. J.; Canonica, L.; Wegelin, M.; Gechter, D.; von Gunten, U. Solar Oxidation and Removal of Arsenic at Circumneutral pH in Iron Containing Waters. *Environ. Sci. Technol.* **2001**, *35* (10), 2114−2121.
(72) McFadden, M.; Giani, R.; Kwan, P.; Reiber, S. H. Contributions to drinking water lead from galvanized iron corrosion scales. *American Water Works Association. Journal* **2011**, *103* (4), 76.

DOI: 10.1021/acs.est.7b04396
Environ. Sci. Technol. 2018, 52, 195−204

(73) Lytle, D. A.; Nadagouda, M. N. A comprehensive investigation of copper pitting corrosion in a drinking water distribution system. *Corros. Sci.* **2010**, *52* (6), 1927−1938.
(74) Katsoyiannis, I. A.; Canonica, S.; von Gunten, U. Efficiency and energy requirements for the transformation of organic micropollutants by ozone, O 3/H 2 O 2 and UV/H 2 O 2. *Water Res.* **2011**, *45* (13), 3811−3822.
(75) Amrose, S. E.; Bandaru, S. R.; Delaire, C.; van Genuchten, C. M.; Dutta, A.; DebSarkar, A.; Orr, C.; Roy, J.; Das, A.; Gadgil, A. J. Electro-chemical arsenic remediation: field trials in West Bengal. *Sci. Total Environ.* **2014**, *488*, 539−546.
(76) Li, L.; van Genuchten, C. M.; Addy, S. E.; Yao, J.; Gao, N.; Gadgil, A. J. Modeling As (III) oxidation and removal with iron electrocoagulation in groundwater. *Environ. Sci. Technol.* **2012**, *46* (21), 12038−12045.
(77) Simeonidis, K.; Papadopoulou, V.; Tresintsi, S.; Kokkinos, E.; Katsoyiannis, I. A.; Zouboulis, A. I.; Mitrakas, M. Efficiency of Iron-Based Oxy-Hydroxides in Removing Antimony from Groundwater to Levels below the Drinking Water Regulation Limits. *Sustainability* **2017**, *9* (2), 238.
(78) Börsig, N.; Scheinost, A. C.; Shaw, S.; Schild, D.; Neumann, T. Uptake mechanisms of selenium oxyanions during the ferrihydrite-hematite recrystallization. *Geochim. Cosmochim. Acta* **2017**, *206*, 236−253.
(79) Pan, C.; Troyer, L. D.; Catalano, J. G.; Giammar, D. E. Dynamics of chromium (VI) removal from drinking water by iron electrocoagulation. *Environ. Sci. Technol.* **2016**, *50* (24), 13502−13510.

DOI: 10.1021/acs.est.7b04396
Environ. Sci. Technol. 2018, 52, 195−204